

# Sensitivity Analysis and Optimal Design of a Dual Mechanical Port Bidirectional Flux-modulated Machine

Yunchong Wang, Shuangxia Niu and Weinong Fu

**Abstract**—This paper presents an optimal design methodology of a dual-mechanical-port bidirectional flux-modulated machine for electric continuously variable transmission (E-CVT) in hybrid electrical vehicles (HEV). The machine utilizes bidirectional flux modulation effect to combine two rotors and one stator together, aiming to realize electrical and mechanical power flexible split and combination. Due to the complexity of the machine structure, conventional optimization methods using analytical model are inapplicable. Therefore, an effective and practical method which combines the genetic algorithm and finite element method (GA-FEM) is proposed to optimize the design of the machine in this paper. Since the computational cost increases exponentially with the increasing of number of design parameters, to reduce the computational cost in the optimization process, the design parameters are divided into two levels basing on a sensitivity analysis. And then the sensitive parameters are optimized using the GA-FEM coupled method. Finally, a prototype is fabricated to verify the effectiveness of the optimal design.

**Index Terms**—E-CVT, dual mechanical port, finite element method, flux modulation, HEV, optimal design.

## I. INTRODUCTION

NOWADAYS, planetary gear unit is widely used in commercial successful hybrid electric vehicles (HEVs), such as Toyota Prius series and Cadillac CT6. The planetary gearbox is a core component of the electronic continuously variable transmission (E-CVT) system in HEVs, which can split and combine the mechanical power from the internal combustion engine (ICE) and the electrical power from battery to drive the wheels efficiently. In Toyota Prius, the ICE couples with the carrier or planetary gear, the sun gear is connected with Motor/Generator I and the ring gear couples with both Motor/Generator II and the final drive. Recently, to reduce maintenance costs and improve the fuel economy, the dual-mechanical-port permanent-magnet (DMP-PM) machine and its application in HEVs have attracted increasing attention

Manuscript received Jan 23, 2017; revised April 14, 2017; accepted June 8, 2017. This work was supported in part by the Research Grant Council, the Hong Kong Special Administrative Region, China, under projects PolyU 152130/14E and 1-ZE5P.

The authors are with The Hong Kong Polytechnic University, Hung Hom, Kowloon, Hong Kong, China (e-mail: wangycee@gmail.com; eesxniu@polyu.edu.hk; eewnfu@polyu.edu.hk). (Corresponding author shuangxia Niu, e-mail: eesxniu@polyu.edu.hk).

[1-4]. The DMP-PM machine proves to be a potential option to substitute the planetary gear unit in E-CVT system. The novel E-CVT system with a DMP-PM machine is more compact, M/G I and M/G II are integrated into one compound machine frame and the planetary gearbox is not required. Compared with the conventional gear box based E-CVT system, the E-CVT system with DMP-PM machine has many advantages, such as high reliability, low mechanical vibration and low audible noise.

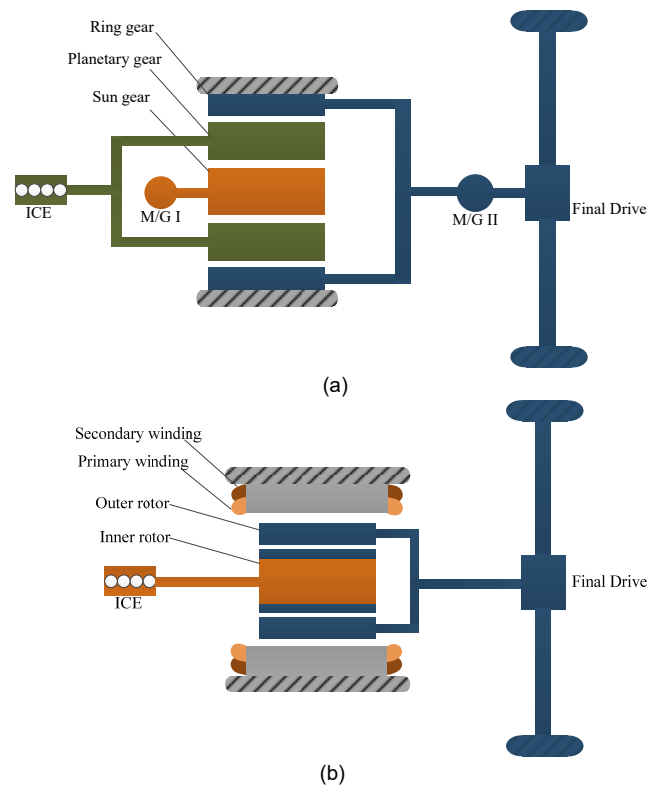


Fig. 1. Basic configuration of the E-CVT systems for HEVs. (a) Planetary gear based E-CVT system. (b) Proposed dual-mechanical-port E-CVT system.

In [3], a PM synchronous dual-rotor machine was presented. In the machine, a PM rotor with 6 poles is sandwiched by a stator and an inner wound rotor. The multi-operational mode of the machine was investigated. Due to the inner wound rotor structure, the brushes and slip rings have to be used in the machine, which brings additional electromagnetic interference and increases the unreliability of the E-CVT system. In [5], a brushless double mechanical port flux-switching PM motor

was designed for HEV application. By placing the stator in the middle of two rotors, this machine eliminates the brushes and slip rings. However, this structure decouples the two rotors and the planetary gearbox is still needed to split and combine the power of the ICE and battery.

To eliminate the brushes, slip rings and the planetary gearbox, a novel structure of DMP-PM machine with flux modulation effect is presented in this paper. The flux modulation effect which is also named as Vernier effect was firstly applied for magnetic gears (MGs) [6]. In the MGs PMs are surface mounted or inset in the inner rotor and the outer rotor, and steel pieces are sandwiched between two rotors to modulate the flux and realize the torque/speed contactless transmission. Extending the concept of MGs to electric machines, a variety of flux modulation machines has been invented [7-14]. In [15] and [16], the flux modulation dual-rotor machine has been investigated. This novel structure integrates two rotors within one machine. The outer rotor with the modulation segments is a PM rotor. Without the wound rotor, this machine can realize the brushless and gearless operation for the HEV application. However, an additional regulating PM machine is still needed to decouple the ICE torque and the wheel torque [16]. To simplify the driven system, a doubly-fed bidirectional-flux-modulation (DF-BFM) machine was presented in [17]. Mounting two sets of windings into one stator, the structure of the DF-BFM is more compact. Due to the relatively complex structure of the DF-BFM, the conventional optimal design which uses the analytical model of the machine is not applicable. Therefore, the multi-level optimization method based on the sensitivity analysis [18-21] is an appropriate option for the design of the DF-BFM. In [5], the multilevel optimization method was used to design a double-mechanical-port flux-switching PM machine. In [22], a V-shaped PM machine was designed with the multi-level method. The parameters are divided into two types, which are significant parameters and non-significant parameters. The response surface method is utilized to determine the optimal values of the significant parameters, and the non-significant parameters are optimized individually.

In this paper the DF-BFM machine is designed to meet the requirements of the HEVs application. The exploded view of the proposed DF-BFM machine is given in Fig. 1 (b). Both the inner rotor and the outer rotor consist of PMs and modulation steels. Two sets of distributed three-phase windings are housed on the stator. The primary winding and two rotors constitute a flux modulation machine, which accounts for the speed and torque distribution between the two rotors. In the HEVs application, the inner rotor is connected with the ICE and the outer rotor is connected with the wheels. Using the flux modulation effect, the primary winding splits and combines the power of the two rotors to ensure the optimal operation of the internal combustion engine (ICE) regardless of the speed variations of the vehicle. The secondary winding and the outer rotor constitute a PM machine, which functions to enhance output torque during acceleration and driving up-hill. Using multi-level optimization method, the DF-FBM machine is optimized. For the significant parameters, the

optimization is realized by using an effective method which combines the finite element method (FEM) and genetic algorithm (GA). GA is a simulated evolutionary optimization method which imitates the natural selection and genetics [23-26]. The non-significant parameters are optimized individually using FEM. The multi-level optimization methodology can effectively reduce the variable numbers of the GA and dramatically decrease the computing time consumption. Finally, a prototype of DF-BFM is fabricated. The effectiveness and correctness are verified by the experimental results.

## II. MOTOR STRUCTURE AND WORKING PRINCIPLE

### A. Motor Structure

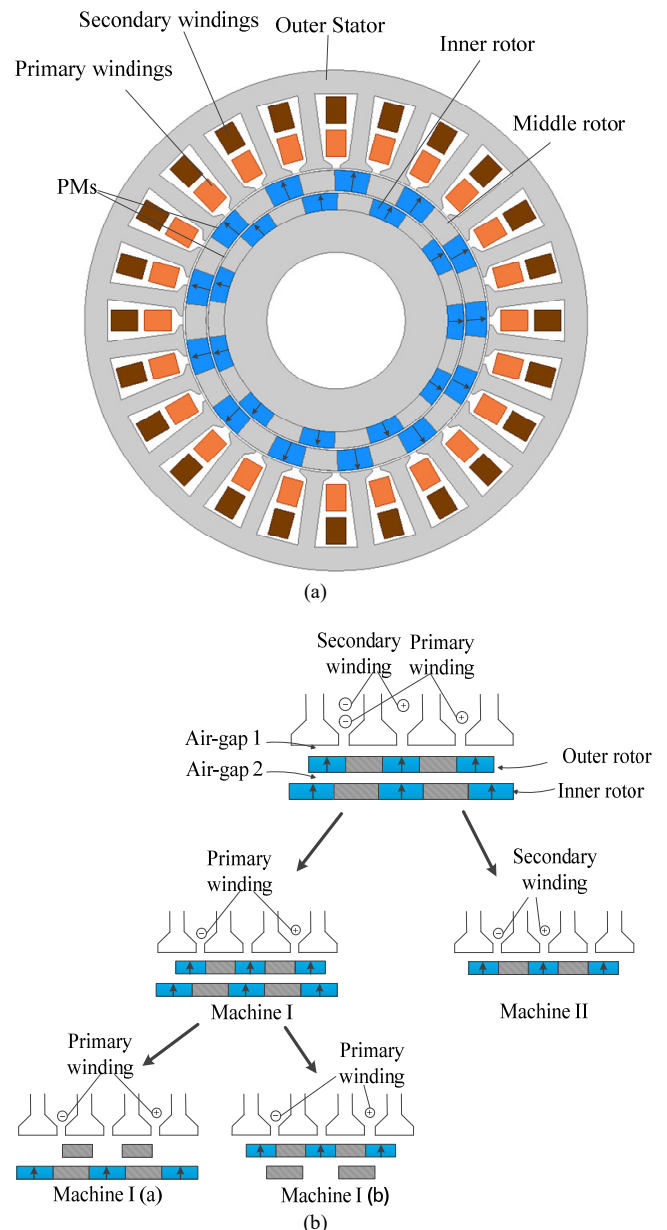


Fig. 2. Basic configuration of the proposed DF-BFM system. (a) Schematic of the DF-BFM. (b) Decomposition of the proposed DR-FBM machine.

Fig. 2 shows the basic configuration of the DF-BFM machine. Two rotors, namely inner rotor and outer rotor, are composed of PM poles and flux modulation segments. Two sets of windings are housed in the outer stator. The primary winding couples with both rotors using the flux-bidirectional-modulation effect. The secondary winding couples with the outer rotor, comprising a conventional PM machine. Basing on the flux modulation effect, the DF-BFM machine can be regarded as a combination of three machines. Machine I is the combination of two flux modulation machines. The field excited by the inner rotor PMs is modulated by the salient poles of the outer rotor and couples with the primary winding and the field excited by the outer rotor PMs is modulated by the salient poles of the inner rotor. The actual field of the primary winding is the sum of the field of Machine I(a) and Machine I(b). Machine II is a conventional PM machine which is comprised of the outer rotor and the secondary winding. Both Machine I(a) and Machine I(b) utilize the flux modulation effect and consist of a bidirectional modulation machine. Using this bidirectional modulation machine, the gearless and brushless structure of DF-BFM machine is constructed.

### B. Working Principle

The basic principle of flux modulation effect is illustrated in [27, 28]. Basing on the flux modulation principle, the general back-EMF of the primary winding is:

$$\begin{aligned} e(t) &= e_a(t) + e_b(t) \\ &= (E_a + E_b) \sin[(N_i \omega_i - N_o \omega_o)t] \end{aligned} \quad (1)$$

where  $e_a$  and  $e_b$  are the back-EMF of the Machine I(a) and Machine I(b).  $E_a$  and  $E_b$  are the amplitude of the  $e_a$  and  $e_b$ , respectively.  $N_i$  and  $N_o$  are the pole-pair numbers of the inner rotor and the outer rotor.  $\omega_i$  and  $\omega_o$  are the mechanical speed of the inner rotor and outer rotor, respectively. It is obvious that the frequency of the primary winding is determined by the rotating speed of both rotors and can be written as:

$$\begin{cases} \omega_p = N_i \omega_i - N_o \omega_o \\ f_p = \frac{\omega_p}{2\pi} = \frac{N_i \omega_i - N_o \omega_o}{2\pi} \end{cases} \quad (2)$$

where  $\omega_p$  is the electrical angular frequency of the primary winding. The torque relationship between the stator and the rotors follow the gear ratio of the planetary gear [16]:

$$T_p : T_{op} : T_i = N_p : (-N_o) : N_i \quad (3)$$

where  $T_p$  is the electromagnetic torque due to the primary winding;  $T_{op}$  is the torque on the outer rotor produced by the major winding and  $T_i$  is the torque on the inner rotor.

Machine II is a conventional PM machine. The frequency of the secondary winding is determined by the rotating speed of

the outer rotor and the electromagnetic torque of the secondary winding equals to the mechanical torque of the outer rotor :

$$\begin{cases} \omega_s = N_o \omega_o \\ f_s = \frac{\omega_s}{2\pi} = \frac{N_o \omega_o}{2\pi} \\ T_s = T_{os} \end{cases} \quad (4)$$

The DF-BFM is a combination of Machine I(a), Machine I(b) and Machine II. The outer rotor couples with both primary winding and secondary winding. Therefore, the actual torque of the outer rotor is:

$$T_o = T_{op} + T_{os} \quad (5)$$

### C. Basic Specification and Initial Design

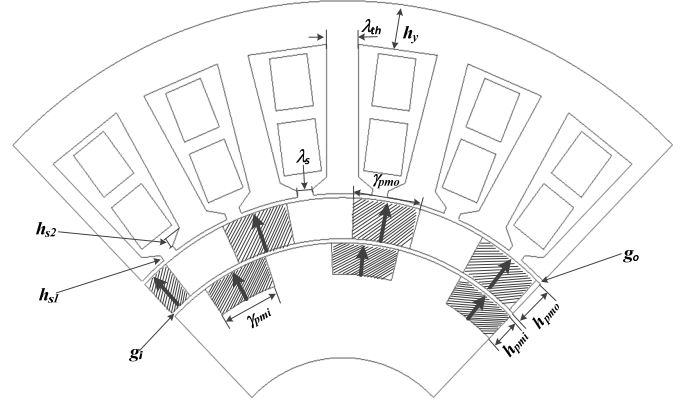


Fig. 3. Parameter model of the proposed DF-BFM machine.

The DF-BFM machine is aimed on the application in the driving system of the HEVs. To meet the requirements of the HEV application, the rated speed of the inner rotor which is connected with the ICE is designed as 2000 rpm to realize the optimal operation of the ICE. The rated speed of the outer rotor which is connected with the wheels is designed as 1000 rpm. Furthermore, to valid the design and optimization method, a 7.5kW prototype of the DF-BFM is manufactured. The specifications and initial design parameters of the prototype are listed in Table I and the geometric parameters of the DF-BFM are shown in Fig. 3. To ensure the feasibility of the fabrication, the geometric parameters need to satisfy some limitations. The air-gap length should be larger than 0.5 mm, the thickness of the stator yoke should be larger than 10 mm and the thickness of the outer rotor should also be larger than 10 mm. The geometric parameters shown in Fig. 3 are the parameters which will be optimized during the design processing. The initial values of these parameters are chosen according to the conventional motor design experience which may not fit for the DF-BFM machine design. Therefore, a further optimization of the DF-BFM machine is carried out before the fabrication of the prototype.

TABLE I  
INITIAL DESIGN PARAMETERS OF THE PROTOTYPE

Item	Value
Rated power (kW)	7.5
Rated speed of inner rotor (rpm)	2000
Rated speed of outer rotor (rpm)	1000
Pole-pair number of the inner rotor	11
Pole-pair number of the outer rotor	13
Pole-pair number of primary winding	2
Pole-pair number of secondary winding	13
Number of stator slots	24
Phase number	3
Turns of primary winding per phase	200
Turns of secondary winding per phase	240
Rated current of primary winding (A)	12
Rated current of secondary winding (A)	8
Axial length (mm)	65
Stator outer diameter (mm)	240
Stator inner diameter (mm)	150
Air-gap length (mm)	1
Inner rotor PM thickness $h_{pmi}$ (mm)	6
Outer rotor PM thickness $h_{pmo}$ (mm)	6
Inner rotor PM width $\gamma_{pmi}$ (°)	14
Outer rotor PM width $\gamma_{pmo}$ (°)	12
Slot opening width $\lambda_s$ (mm)	2.5
Slot opening height $h_{s1}$ (mm)	1 mm
Slot wedge height $h_{s2}$ (mm)	2 mm
Tooth width $\lambda_{th}$ (mm)	8
Stator yoke thickness (mm)	15 mm
Magnetic remanence (T)	1.2

### III. MACHINE DESIGN AND OPTIMIZATION

Due to the complexity of the DF-BFM machine, the conventional optimization using analytical method is inaccurate and difficult to realize the optimization of DF-BFM. The GA method combined with FEM (GA-FEM) is proposed in this paper. The merit of this methodology is that it can optimize the machine with enough accuracy. However, the computing time of this methodology increases dramatically with the increasing of the optimizing parameters. As mentioned before, the DF-BFM machine can be divided into two machines, Machine I, Machine II. These two machines share the same outer rotor and the stator. Therefore, it is unreasonable to optimize these two machines separately. However, it takes too much time to optimize all the parameters using the GA-FEM methodology. To reduce the computing time consumption, the geometric parameters are classified as two levels based on the sensitivity analysis. For the optimization sensitive parameters, the GA-FEM method is employed. Then, the non-sensitive parameters are optimized individually. The flow chart of the optimization is shown in Fig. 4.

#### A. Optimization Model

The DF-BFM machine is applied for the E-CVT system of HEVs. Basing on the requirements of the E-CVT system, the objective function of the optimization is selected. The objective function can be written as:

$$O(\mathbf{x}_i) = \max\{w_1 T_{I_{max}}(\mathbf{x}_i) + w_2 T_{II_{max}}(\mathbf{x}_i)\} \quad (6)$$

where  $T_{I_{max}}$ , the maximum torque of Machine I, is a key performance factor for the DF-BFM machine and determines the power transmission capability of the DF-BFM machine between the ICE and the wheels.  $T_{II_{max}}$  is the maximum torque of the Machine II and represents the start-up and acceleration capability of the system.  $w_1$  and  $w_2$  are the weight coefficients. The weight coefficients show the importance level of each performance index. Considering the application of the DF-BFM machine, the power transmission capability is more important, the value of  $w_1$  is set as 0.7 and  $w_2$  is 0.3.  $\mathbf{x}_i$  is the vector of the optimization parameters and can be written as:

$$\mathbf{x}_i = [x_1 \ x_2 \ x_3 \ x_4 \ x_5 \ x_6 \ x_7 \ x_8 \ x_9 \ x_{10} \ x_{11}]^T \\ = [h_{pmi} \ h_{pmo} \ h_y \ h_{s1} \ h_{s2} \ \lambda_{th} \ \lambda_s \ \gamma_{pmi} \ \gamma_{pmo} \ g_i \ g_o]^T \quad (7)$$

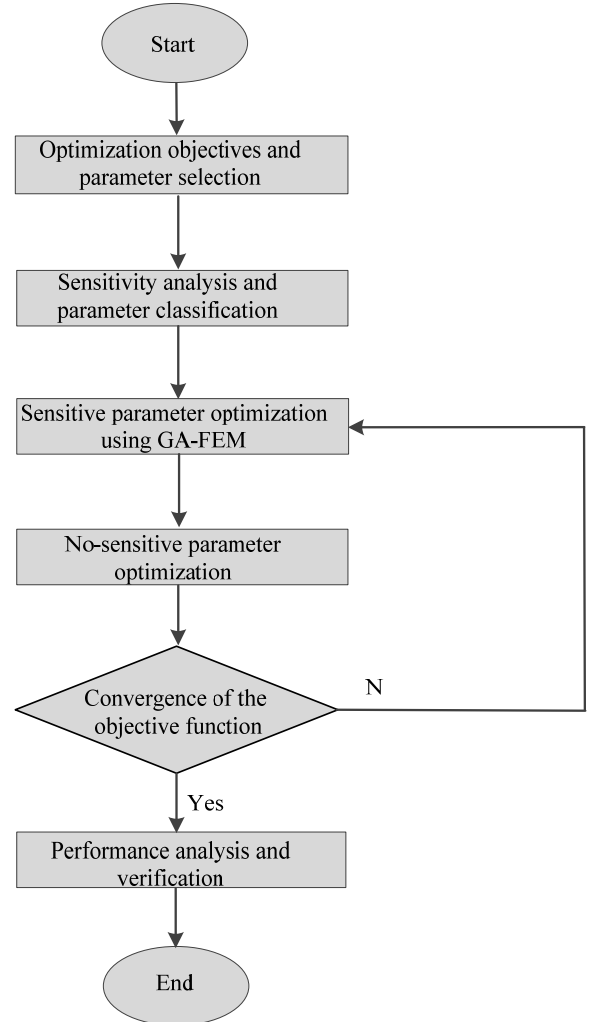


Fig. 4. The flowchart of the optimization.

To guarantee the reliability of the mechanical structure and avoid the conflict of the geometric size, the boundaries of the parameters are listed as:

$$\left. \begin{aligned}
 &2\text{mm} \leq h_{pmi} \leq 20\text{mm} \\
 &10\text{mm} \leq h_{pmo} \leq 20\text{mm} \\
 &10\text{mm} \leq h_y \leq 30\text{mm} \\
 &1\text{mm} \leq h_{s1} \leq 5\text{mm} \\
 &1\text{mm} \leq h_{s2} \leq 5\text{mm} \\
 &3\text{mm} \leq \lambda_{th} \leq 15\text{mm} \\
 &2\text{mm} \leq \lambda_s \leq 5\text{mm} \\
 &5^\circ \leq \gamma_{pmi} \leq 20^\circ \\
 &5^\circ \leq \gamma_{pmo} \leq 20^\circ \\
 &0.6\text{mm} \leq g_o \leq 3\text{mm} \\
 &0.6\text{mm} \leq g_i \leq 3\text{mm}
 \end{aligned} \right\} \quad (8)$$

### B. Sensitivity Analysis

To reduce the computation cost required for the GA-FEM optimization, the parameters are divided into two classes based on the sensitivity analysis, namely the sensitive parameters and non-sensitive parameters. The sensitivity reveals the correlation ship between the parameter and the objective. Regardless the interaction effects among the parameters, the sensitivity of a parameter shows its effect on value of the objective function. The selection of the initial design of the DF-BFM machine is important for the accuracy of the sensitivity analysis.

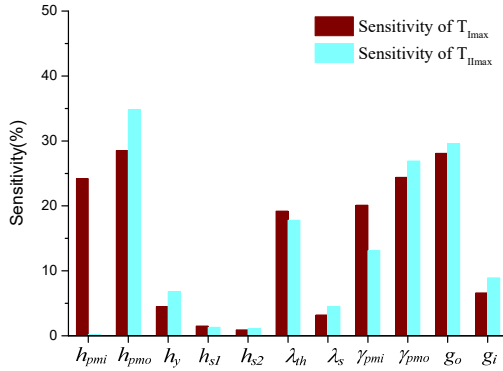


Fig. 5. Sensitivity of indices of  $T_{max}$  and  $T_{llmax}$

TABLE II  
SENSITIVITY INDICES OF  $S_o$

Design Parameter	Sensitivity $S_o$ (%)
$h_{pmi}$	17.05
$h_{pmo}$	30.39
$h_y$	5.19
$h_{s1}$	1.45
$h_{s2}$	0.96
$\lambda_{th}$	18.78
$\lambda_s$	3.59
$\gamma_{pmi}$	18.11
$\gamma_{pmo}$	25.15
$g_o$	28.55
$g_i$	7.29

TABLE III  
PARAMETER CLASSIFICATION BASING ON THE SENSITIVITY

Level	Design parameters
Non-sensitive parameters	$h_y, h_{s1}, h_{s2}$ $\lambda_s, g_i$
Sensitive parameters	$h_{pmi}, h_{pmo}, \lambda_{th}$ $\gamma_{pmi}, \gamma_{pmo}, g_o$

In order to measure the sensitivity of the parameters, the sensitivity index can be expressed as:

$$S(x_j) = \frac{x_{j0}}{O(x_0)} \cdot \frac{\partial O}{\partial x_j} \Big|_{x_i=x_0} \square \frac{\Delta O / O(x_0)}{\Delta x_j / x_{j0}} \quad (9)$$

where  $x_j$  is the parameter which is measured,  $x_0$  is the initial design of the DF-BFM machine. Basing on the motor design experience and FEM analysis results, the initial design of the DF-BFM machine is selected as shown in Table I.

From (6), the objective function of the optimization of the DF-BFM machine is composed of two components,  $T_{Imax}$  and  $T_{llmax}$ . The comprehensive sensitivity  $S_o$  can be defined as:

$$S_o = w_1 |S_{T_{Imax}}(x_i)| + w_2 |S_{T_{llmax}}(x_i)| \quad (10)$$

( $w_1 = 0.7, w_{ll} = 0.3$ )

The sensitivities of the  $T_{Imax}$  and  $T_{llmax}$  to the 11 parameters are calculated by (9) and are shown in Fig. 5 and the comprehensive sensitivity  $S_o$  to the 11 design parameters are listed in Table II.

Basing on the sensitivities, the design parameters are divided into two levels:

$$\begin{cases}
 \text{Non-Sensitive Parameters} : S_o < 10\% \\
 \text{Sensitive Parameters} : S_o \geq 10\%
 \end{cases} \quad (11)$$

As shown in Table III, the sensitive parameters include  $h_{pmi}$ ,  $h_{pmo}$ ,  $\lambda_{th}$ ,  $\gamma_{pmi}$ ,  $\gamma_{pmo}$ ,  $g_o$ . The sensitivities of these parameters are obviously larger than those of other parameters which means these parameters own much higher effects on the value of the objective function than the non-sensitive parameters. In the optimization of sensitive parameters, the GA-FEM method is employed. The computational cost of the GA-FEM optimization is reduced dramatically by decreasing the parameter number from 11 to 6.

### C. Optimization of the Sensitive Parameters

The GA-FEM method is a combination of the GA and FEM, the flow chart of this method is shown in Fig. 6. GA is a search method which simulates the nature's biological evolution. Using selection, crossover and mutation, GA starts at an initial population and moves from one population to another population.

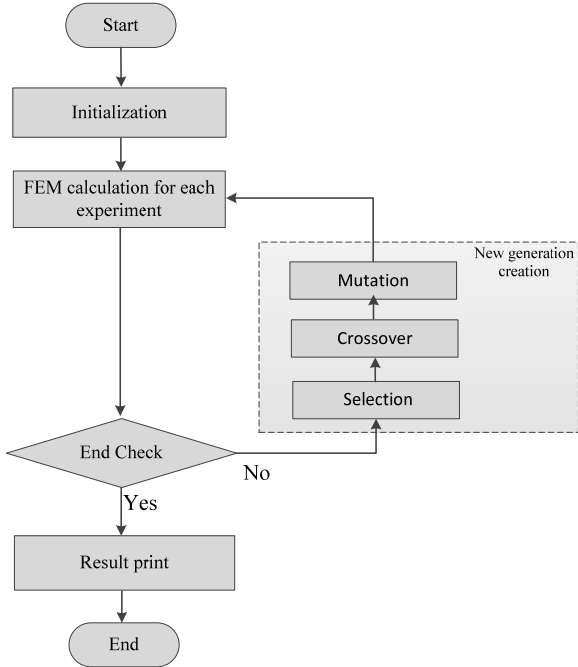


Fig. 6. The flowchart of the GA-FEM methodology.

The population is an assembly of elements which are calculated by a numerical experiment using FEM analysis. The number of elements in each population is named as population size. As a trade-off between accuracy and computational cost, the population size is set as 40. The initial population is generated randomly at the beginning of the algorithm. Each element owns a fitness value which is calculated using FEM and the fitness function is the same as the objective function shown in (10). The fitness value is used to judge the ending of the GA. The end condition is written as:

$$\frac{|F_i - F_{i-5}|}{5} \leq \varepsilon \quad (i \leq \text{generation size}) \quad (12)$$

where  $F_i$  and  $F_{i-5}$  are the best fitness value of the  $i^{\text{th}}$  generation and  $(i-5)^{\text{th}}$  generation.  $(F_i - F_{i-5})/5$  is the average value of the fitness error of the last five generation. The fitness value also determines the survival rate of an element. The survival rate of an element is in proportion to its fitness value in the selection function. During the selection function, a new population is generated according to the fitness value of the elements of last population. In the selection process, the best element with highest fitness value survives and the worst element is eliminated. It guides the population evolve towards better solutions. After the generation of a new population, crossover and mutation operate on the new populations. The reproduced offspring solutions are created by these operators to realize the evolution process of the algorithm. Fig. 7 shows the search result of GA optimization. It is obvious that the objective value raises rapidly at the beginning of the algorithm and converge to an optimization point after 24 generations. The optimization results of the sensitivity parameters are listed in Table IV.

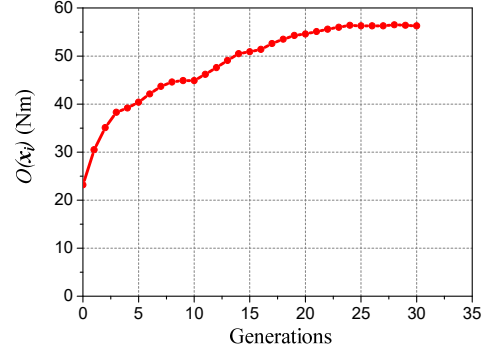


Fig. 7. The search result of the GA optimization.

TABLE IV  
OPTIMIZATION RESULT OF THE SENSITIVE PARAMETERS

Design Parameter	Optimal Value
$h_{pmi}$	7.68mm
$h_{pmo}$	10.59mm
$\lambda_{th}$	7.52mm
$\gamma_{pmi}$	16.37°
$\gamma_{pmo}$	13.84
$g_o$	0.6mm

#### D. Optimization of the Non-sensitive Parameters

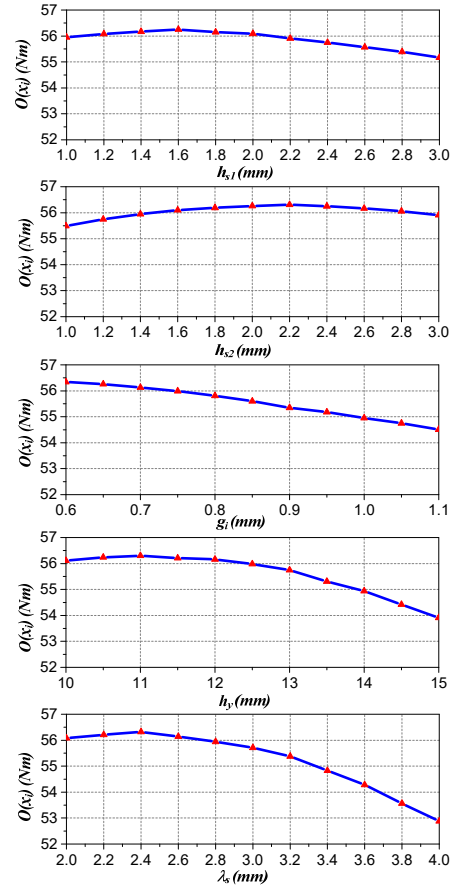


Fig. 8. The comprehensive Objective  $O(x_j)$  as the functions of the non-sensitive parameters.

TABLE V  
OPTIMIZATION RESULT OF THE NON-SENSITIVE PARAMETERS

Design Parameter	Optimal Value
$h_{s1}$	1.5mm
$h_{s2}$	2.1mm
$h_p$	11mm
$g_i$	0.6mm
$\lambda_s$	2.4mm

Due to the small sensitivities, the interaction effects of the non-sensitive parameters are neglected and the non-sensitive parameters are optimized individually. Fig. 8 shows the objective  $S_O$  as the function of the non-sensitive parameters. As the aforementioned analysis, the effects of these non-sensitive parameters on the objective function value are non-significant. The optimization results are listed in the Table V.

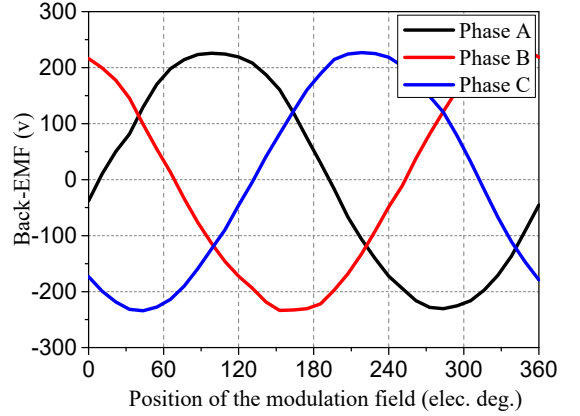
#### IV. PROTOTYPE ANALYSIS AND EXPERIMENTAL RESULTS

##### A. FEM Simulation

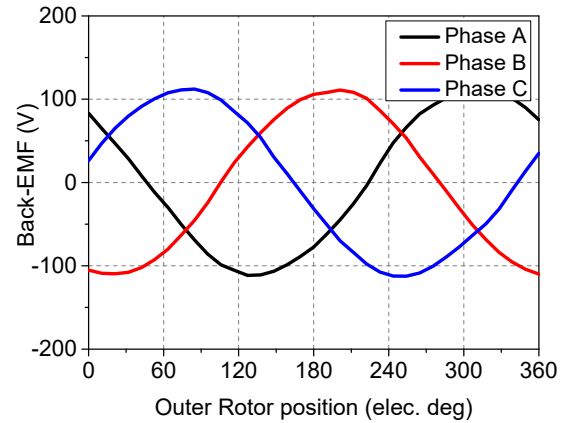
Basing on the optimization result, the electromagnetic performance of the prototype is simulated using FEM analysis. The no-load flux-line distribution of the optimal DF-BFM is shown in Fig. 9. The two pole-pair magnetic field of the stator which is excited by the two rotors with the modulation effect is conspicuous. This field coupled with the primary winding with two pole pairs is utilized to realize the power split and combination of the inner rotor connected with the ICE. The no-load back-EMFs of the two windings are shown in Fig. 10. The simulation condition is that the inner rotor rotates at rated speed, 2000 rpm and the outer rotor rotates at 1000 rpm. The DF-BFM machine employs the modulation effects which use the field harmonics to transfer power. Comparing with the conventional PM synchronous machines, the total harmonic distortion (THD) of the DF-BFM is a little larger. The total THD of the primary winding is 2.17% and the secondary winding THD is 2.43%.



Fig. 9. The no-load flux-line distribution of the optimal DF-BFM.



(a)



(b)

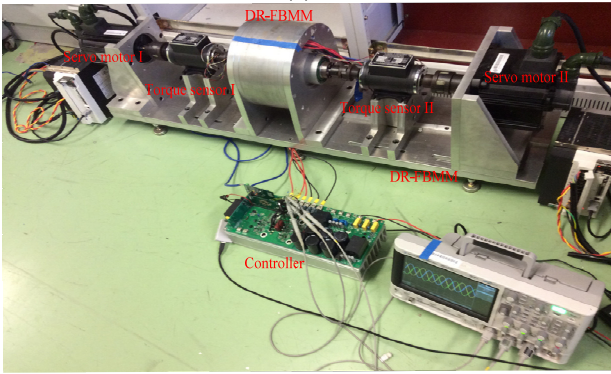
Fig. 10. Simulation of the no-load back-EMF. (a) The primary winding. (b) The secondary winding.

##### B. Experimental Validation

To verify the validity of the DF-BFM machine and the simulation results, a prototype of the DF-BFM machine is manufactured, as shown in Fig. 11. The parameters of the prototype are designed according to the optimization results. To verify the performance of the prototype, a test bench is built using two sets of servo systems which are connected with two rotors respectively. The servo system connected with the inner rotor simulates the function of the ICE of the HEVs and the other servo system coupled with the outer rotor is used to simulate the load condition of the wheels. Fig. 12 shows the no-load back-EMF waveforms under rated rotor speeds. The experimental results are in agreement with the simulation results shown in Fig. 10. Due to the axial flux leakage which is not considered in the 2D-FEM simulation, the amplitude of the experimental waveform of the primary no-load back-EMF is 8% percent smaller than the simulation results. In case of secondary winding, the axial flux leakage is much smaller. The secondary winding only couples with the outer rotor. Hence, the flux leakage of the secondary winding is largely caused by the end region.

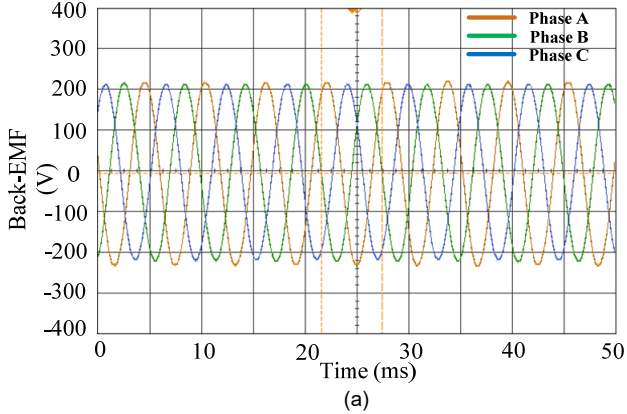


(a)

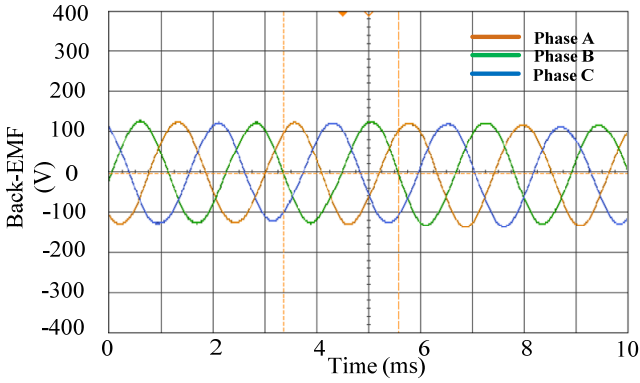


(b)

Fig. 11. Photograph of the DF-FBM machines. (a) Machine prototype. (b) Test bench.



(a)



(b)

Fig. 12. Experimental waveform of the no-load back-EMF. (a) The primary winding. (b) The secondary winding.

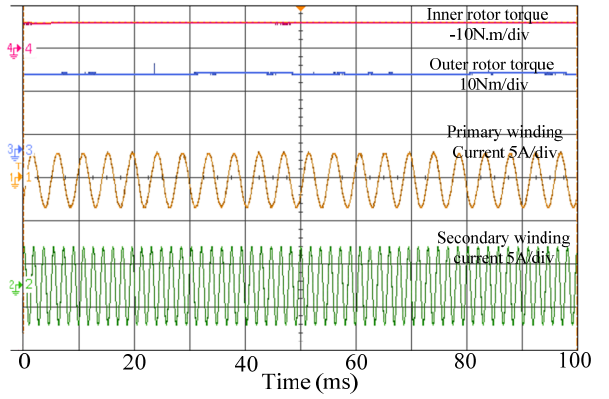


Fig. 13. Experimental waveform of steady-state torque.

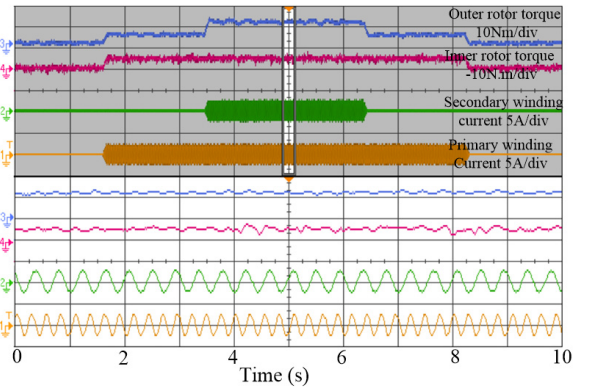


Fig. 14. Experimental waveform of dynamic performance.

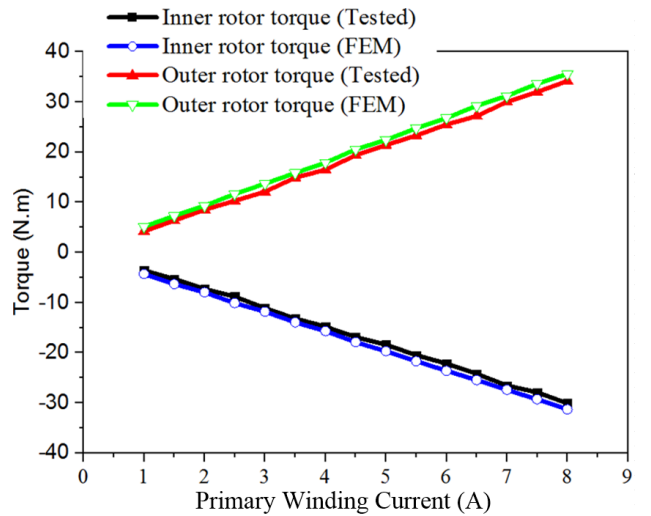


Fig. 15. Experimental waveform of dynamic performance.

The steady-state torque and current waveform are shown in the Fig. 13. The primary winding current is 2 A and the secondary winding current is 5 A. The inner rotor torque is 7.3 Nm and the outer rotor torque is 18.4 Nm. Both windings are fed from 3-phase inverters using a common DC bus. Fig. 14 shows dynamic performance of the DF-FBM machine. At 1.6s, the primary winding current steps to 2A. Consequently, the inner rotor torque steps to 7.3Nm and the outer rotor torque steps to 8.6Nm. At 3.5s, the secondary winding current steps to 2.5A. Due to the decoupling between the inner rotor and the secondary winding, the inner rotor torque is unaffected by the

secondary winding and the outer rotor torque steps to 14.2Nm. Fig. 15 shows the torque of two rotors with different primary winding current. It can be seen that the experimental results agree well with the FEM simulation results and the torque distribution between the two rotors is in agreement with the theoretical analysis. The small discrepancy between the experimental result and simulation result is caused by the end effect and the mechanical loss of the prototype.

The rotor field-orientation control (FOC) strategy is applied on both windings. The control strategy is not the focus of this paper and will be discussed in detail in the further paper.

TABLE VI  
LOSS AND EFFICIENCY AT DIFFERENT PRIMARY WINDING FREQUENCY

Primary winding frequency (Hz)	Core loss (W)	Copper loss (W)	No-load loss (W)	Output power of outer rotor (kW)	Efficiency (%)
0	10.13	83.81	18.24	1.89	94.4
50	42.76	83.56	19.17	2.41	94.2
100	104.65	83.54	19.89	2.93	93.3
150	208.51	83.49	20.91	3.45	91.7
200	381.42	83.76	22.63	3.97	89.1

TABLE VII  
LOSS AND EFFICIENCY AT DIFFERENT SECONDARY WINDING FREQUENCY

Secondary winding frequency (Hz)	Core loss (W)	Copper loss (W)	Mechanical loss (W)	Output power of outer rotor (kW)	Efficiency (%)
50	5.14	30.48	8.92	0.24	84.5
100	10.42	30.57	9.36	0.47	90.2
150	19.63	30.16	9.98	0.70	91.9
200	37.12	30.33	10.92	0.94	92.1
250	70.83	30.55	11.88	1.18	92.3

Due to the decoupling of the Machine I and Machine II, the losses of Machine I and Machine II can be considered individually. For the Machine I, the frequency of the primary winding is determined by the speed difference of the two rotors and the core loss increased dramatically as the primary winding frequency. Table VI lists the loss and efficiency of Machine I with different primary winding frequency. The current of the primary winding is 5A and the inner rotor speed is fixed at 1000rpm. For the Machine II, it is a conventional PM machine, the loss and efficiency are listed in Table VII. During the test, the secondary winding current is 5A and the inner rotor is stationary.

## V. CONCLUSION

In this paper, an optimal design method for a dual mechanical port machine with flux modulation effect is presented. The working principle of the DF-BFM machine is illuminated firstly. Due to the complexity structure of the machine, conventional optimization method with analytical model is inapplicable for the DF-BFM machine. Therefore, GA-FEM optimization methodology is proposed. To reduce computational cost, the design parameters are divided into two levels basing on the sensitivity analysis results. The sensitivity analysis reveals the relationship between the parameters and the objective function. In the optimization design of the sensitive parameters, GA-FEM method is employed. And then the electromagnetic performance of the prototype is analyzed.

Finally, a prototype machine is fabricated. The experimental results verify the validity of the machine operation principle and optimal design method. The GA-FEM methodology with sensitivity analysis is proved to be an effective and practical optimization method for design of novel machines with complex structures.

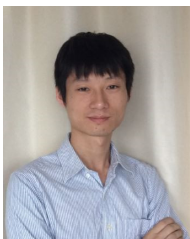
## REFERENCES

- [1] K. T. Chau, C. C. Chan, and C. Liu, "Overview of permanent-magnet brushless drives for electric and hybrid electric vehicles," *IEEE Trans. Ind. Electron.*, vol. 55, no. 6, pp. 2246–2257, Jun. 2008.
- [2] J. Druant, H. Vansompel, F. D. Belie, J. Melkebeek and P. Sergeant. "Torque analysis on a double rotor electrical variable transmission with hybrid excitation," *IEEE Trans. Ind. Electron.*, vol. 64, no. 1, pp. 60–68, Jan. 2017.
- [3] L. Xu, Y. Zhang, and X. Wen, "Multioperational modes and control strategies of dual-mechanical-port machine for hybrid electrical vehicles," *IEEE Trans. Ind. Appl.*, vol. 45, no. 2, pp. 747–755, Mar./Apr. 2009.
- [4] S. Niu, S. L. Ho and W. N. Fu, "A novel double-stator double-rotor brushless electrical continuously variable transmission system," *IEEE Trans. Magn.*, vol. 49, no. 7, pp. 3909–3912, July. 2013.
- [5] Z. Xiang, X. Zu, L. Quan, Y. Du, C. Zhang and D. Fan, "Multilevel design optimization and operation of a brushless double mechanical port flux-switching permanent-magnet motor," *IEEE Trans. Ind. Electron.*, vol. 63, no. 10, pp. 6042–6054, Oct. 2017.
- [6] K. Atallah, S. D. Calverley, and D. Howe, "Design, analysis and realisation of a high-performance magnetic gear," *Inst. Electr. Eng. Proc. Electr. Power Appl.*, vol. 151, no. 2, pp. 135–143, Mar. 2004.
- [7] S. L. Ho, S. Niu, and W. N. Fu, "Design and Comparison of Vernier Permanent Magnet Machines," *IEEE Trans. Magn.*, Vol. 47, No. 10, pp. 3280–3283, Oct. 2011.
- [8] K. T. Chau, D. Zhang, J. Z. Jiang, C. Liu and Y. Zhang, "Design of a magnetic-g geared outer-rotor permanent-magnet brushless machine for electric vehicles," *IEEE Trans. Magn.*, vol. 43, no. 6, pp. 2504–2506, Jun. 2007.
- [9] Y. Oner, Z. Q. Zhu, L. J. Wu, X. Ge, Hanlin Zhan and J. T. Chen, "Analytical on-load subdomain field model of permanent-magnet Vernier machines," *IEEE Trans. Ind. Electron.*, vol. 63, no. 7, pp. 4105–4117, Feb. 2016.
- [10] Y. Fan, L. Zhang, M. Cheng and K. T. Chau, "Sensorless SVPWM-FADTC of a new flux-modulation permanent-magnet wheel motor based on a wide-speed sliding mode observer," *IEEE Trans. Ind. Electron.*, vol. 62, no. 5, pp. 3143–3151, Dec. 2014.
- [11] S. L. Ho, S. Niu and W. N. Fu, "Design and analysis of a novel axial-flux electric machine," *IEEE Trans. Magn.*, vol. 47, no. 10, pp. 4368–4371, Sep. 2011.
- [12] L. Xu, G. Liu, W. Zhao, X. Yang and R. Cheng, "Hybrid stator design of fault-tolerant permanent-magnet Vernier machines for direct-drive applications," *IEEE Trans. Ind. Electron.*, vol. 64, no. 1, pp. 179–190, Jan. 2017.
- [13] D. Li, R. Qu, and T. Lipo, "High power factor vernier permanent magnet machines," *IEEE Trans. Ind. Appl.*, vol. 50, no. 6, pp. 3664–3674, Nov./Dec. 2014.
- [14] W. Zhao, J. Zheng, J. Wang, G. Liu, J. Zhao, Z. Fang, "Design and Analysis of a Linear Permanent- Magnet Vernier Machine With Improved Force Density," *IEEE Trans. Ind. Electron.*, vol. 63, pp. 2072–2082, Apr. 2016.
- [15] L. Sun, M. Cheng, and H. Jia, "Analysis of a novel magnetic-g geared dual rotor motor with complementary structure," *IEEE Trans. Ind. Electron.*, vol. 62, no. 11, pp. 6737–6747, Nov. 2015.
- [16] J. Bai, P. Zheng, C. Tong, Z. Song and Q. Zhao, "Characteristic analysis and verification of the magnetic-field modulated brushless double-rotor machine", *IEEE Trans. Ind. Electron.*, vol. 62, no. 7, pp. 4023–4033, Jul. 2015.
- [17] S. Niu, S. L. Ho, and W. N. Fu, "Design of a novel electrical continuously variable transmission system based on harmonic spectra analysis of magnetic field," *IEEE Trans. Magn.*, vol. 49, no. 5, pp. 2161–2164, May 2013.
- [18] G. Lei, C. Liu, J. Zhu, Y. Guo, "Techniques for multilevel design optimization of permanent magnet motors," *IEEE Trans. Energy Convers.*, vol. 30, no. 4, pp. 1574–1584, Dec. 2015.

- [19] Y. Tang, P. Ju, H. He, C. Qin, and F. Wu, "Optimized control of DFIG-based wind generation using sensitivity analysis and particle swarm optimization," *IEEE Trans. Smart Grid.*, vol. 4, no. 1, pp. 509–520, Mar. 2013.
- [20] J. G. Amoros, P. Andrada, "Sensitivity analysis of geometrical parameters on a double-sided linear switched reluctance motor," *IEEE Trans. Ind. Electron.*, vol. 57, no. 1, pp. 311–319, Jan. 2010.
- [21] C. Ma, L. Qu, "Multiobjective optimization of switched reluctance motors based on design of experiments and particle swarm optimization," *IEEE Trans. Energy Convers.*, vol. 30, no. 3, pp. 1144–1153, Sep. 2015.
- [22] X. Zhu, Z. Shu, L. Quan, Z. Xiang and X. Pan, "Multi-objective optimization of an outer-rotor V-shaped permanent magnet flux switching motor Based on multi-level Design method," *IEEE Trans. Magn.*, vol. 52, no. 10, pp. 1–1, Oct. 2016.
- [23] J. A. Vasconcelos, J. A. Ramirez, R. H. C. Takahashi, R. R. Saldanha, "Improvements in genetic algorithms," *IEEE Trans. Magn.*, vol. 37, no. 5, pp. 3414–3417, Sep. 2001.
- [24] H. M. Hasanien, A. S. Abd-Rabou, S. M. Sakr, "Design optimization of transverse flux linear motor for weight reduction and performance improvement using response surface methodology and genetic algorithms," *IEEE Trans. Energy Convers.*, vol. 25, no. 3, pp. 598–605, Sep. 2010.
- [25] T. Ishikawa, K. Nakayama, N. Kurita, F. P. Dawson, "Optimization of rotor topology in PM synchronous motors by genetic algorithm considering cluster of materials and cleaning procedure," *IEEE Trans. Magn.*, vol. 50, no. 2, Feb. 2014.
- [26] S. L. Ho, S. Yang and W. N. Fu, "A population-based incremental learning vector algorithm for multiobjective optima designs," *IEEE Trans. Magn.*, vol. 47, no. 5, pp. 1306–1309, May. 2011.
- [27] B. Kim and T. A. Lipo, "Operation and Design Principles of a PM Vernier Motor," *IEEE Trans. Ind. Appl.*, Vol. 46, No. 6, pp. 3656–3663, Sept. 2014.
- [28] L. Sun, M. Cheng, H. Jia, and L. Song, "Analysis and Control of Complementary Magnetic-Gear Dual-Rotor Motor," *IEEE Trans. Ind. Electron.*, vol. 63, no. 11, pp. 6715–6725, Jun. 2016.



**W. N. Fu** received his BEng in Electrical Engineering, Hefei University of Technology, Hefei, China in 1982 and MEng in Electrical Engineering, Shanghai University of Technology, Shanghai, China in 1989. He obtained his PhD in electrical engineering from The Hong Kong Polytechnic University in 1999. He is now a Professor in The Hong Kong Polytechnic University. Before joining the university in October 2007, he was one of the key developers at Ansoft Corporation in Pittsburgh, USA. He has about seven years of working experience at Ansoft, focusing on the development of the commercial software Maxwell. He has published 184 papers in refereed journals. His current research interests mainly focus on numerical methods of electromagnetic field computation, optimal design of electric devices based on numerical models, applied electromagnetics and novel electric machines.



**Yunchong Wang** received his B.Sc and M.Sc degrees, from the school of Electrical Engineering, Zhejiang University, Zhejiang, China, in 2010 and 2013, respectively. He is currently working toward the Ph.D. degree in the department of Electrical Engineering from The Hong Kong Polytechnic University. His research interests include electrical motor design and control, electrical vehicles and renewable energy conversion system.



**Shuangxia Niu** received the B.Sc. and M.Sc. degrees, from the School of Electrical Engineering and Automation, Tianjin University, Tianjin, China, in 2002 and 2005, respectively, and the Ph.D. degree from the Department of Electrical and Electronic Engineering, The University of Hong Kong, Hong Kong, in 2009. Since 2009, she has been with The Hong Kong Polytechnic University, where she is currently an Assistant Professor in the Department of Electrical Engineering. She has authored or coauthored over 70 conference papers and more than 50 papers in leading journals. Her research interests include the design and control of novel electrical machines and drives, renewable energy conversion system and applied electromagnetics..